Available online at www.sciencedirect.com

SciVerse ScienceDirect

Procedia IUTAM 5 (2012) 124 – 133

Procedia IUTAM

www.elsevier.com/locate/procedia

IUTAM Symposium on 50 Years of Chaos: Applied and Theoretical

Analysis of ILM Logic Operations via van der Pol Phase Planes

M. Sato[a]*, Y. Takao[a], N. Fujita[a], S. Imai[a], S. Nishimura[a], W. Shi[a], Y. Soga[a] and A. J. Sievers[b]

[a]*Graduate School of Natural Science and Technology, Kanazawa University, Kanazawa, Japan*
[b]*Laboratory of Atomic and Solid State Physics, Cornell University, Ithaca NY, USA*

Abstract

Logic operations that have previously been numerically demonstrated using intrinsic localized modes (ILMs) in a driven nonlinear 1-D lattice are analyzed using van der Pol phase planes. The time dependent application of a vibrational impurity mode either can produce or destroy an ILM. The appearance or absence of the resulting ILM can be understood via trajectories in the phase plane controlled by the evolving attractors associated with the time dependent impurity mode. Switching between the two possible branches depends on the phase of the amplitude modulation when the impurity mode is removed.

Keywords: Intrinsic Localized mode; van der Pol phase plane; logic operation

1. Introduction

Micro-electro-mechanical systems (MEMS) now have a variety of applications.[1-3] With the continuing decrease in size the nonlinear vibrational properties of such MEMS resonators can no longer be ignored. To this end we have studied driven 1-D micromechanical nonlinear lattices. A general dynamical feature of such a lattice, that only depends on discreteness and nonlinearity, is an intrinsic localized mode (ILM), a dynamically localized excitation that for positive nonlinearity can appear above the plane wave frequency band. [4-8] Because of damping a driver is required to maintain a steady state ILM.[9-15] Such a steady state excitation can be generated by chirping the frequency of the driver beyond

* Corresponding author. Tel.: +81-76-276-6077; fax: +81-76-276-6739.
E-mail address: msato153@staff.kanazawa-u.ac.jp.

 doi:10.1016/j.piutam.2012.06.015

the range of the plane wave spectrum and maintained at that frequency with a cw oscillator of constant amplitude.[16] These driver locked ILMs are self sustained localized oscillations and are stationary stable. It can be moved from one lattice site to another by introducing a mobile impurity into the lattice.[17] When an autoresonant[18] ILM is near an impurity mode it releases some amplitude and becomes trapped at the impurity mode site; on the other hand, if the impurity mode is removed the ILM recovers its intrinsic amplitude. These features suggested that this excitation may be attractive for information processing. Starting from this idea we carried out numerical simulations introducing a spatially inhomogeneous, harmonic force constant, time dependent perturbation into the nonlinear lattice to control ILMs that are locked to the driver. We found that ILMs could be produced or destroyed and the existence or absence of such an ILM was then coded to logic "1" or "0". By the application of such a timed disturbance to the 1-D cantilever array an inverter and NOR operation were demonstrated.

In this paper we show that an impurity mode trajectory in the van der Pol phase plane can be used to determine the correct time dependent application of a spatial impurity pattern to either produce or destroy an ILM. The appearance or absence of an ILM can be understood via paths in the phase plane controlled by evolving attractors driven by the time dependent impurity pattern. The next section focuses on the necessary background material. Section 3 makes contact with the van der Pol phase plane application. The results are summarized in Section 4.

2. Background

2.1. Equations of motion

We have used a simulation lattice model based on experiments. The experimental array is composed of one long and one short cantilever in a unit cell so that the highest frequency optic mode of this di-element lattice can be excited uniformly by a PZT attached to the sample. The equations of motion for the simulations are

$$\begin{aligned} & m_i \frac{d^2 x_i}{dt^2} + \frac{m_i}{\tau}\frac{dx_i}{dt} + k_{2Oi}x_i + k_{4O}x_i^3 + \sum_j k_{2I}^{(j)}\left(2x_i - x_{i+j} - x_{i-j}\right) \\ & + k_{4I}\left\{\left(x_i - x_{i+1}\right)^3 + \left(x_i - x_{i-1}\right)^3\right\} = m_i \alpha \cos\Omega t \end{aligned} \tag{1}$$

where i is the site number of the cantilever, m_i is the mass, τ is the relaxation time, k_{2Oi} and k_{4O} are harmonic and quartic onsite spring constant, $k_{2I}^{(j)}$ is the harmonic spring constant for the intersite connection up to j-th neighbor, and k_{4I} is the quartic spring constant for the intersite connection. The right hand side is the driving term. Parameters, listed in Table II, Ref. [16], are estimated from experimental data of the cantilever array. The driving parameters are $\Omega/2\pi$=139 kHz and α=500 m/s^2.

To produce an ILM at a specific lattice location and frequency the driver is set to the desired frequency and a lattice defect is introduced at that site in the array so that it produces a linear defect mode above the top of the band. In simulations, this is achieved by changing the onsite harmonic spring constant k_{2Oi} locally. The defect pattern is shown in Fig. 1(a). It generates many impurity modes above the regular band mode as shown in Fig. 1(b). The strength of the defect array is increased with time as shown in Fig. 1(c) until the highest frequency impurity mode coincides with the driver frequency. The resultant signal, shown in Fig. 1(d), first appears as an amplitude modulated vibration because of the transient initiation. When the impurity array is removed at the same rate the ILM remains, as shown in Fig. 1(d). This process is similar to the seeding process described in Ref. [16], where one impurity with a time dependent

impurity strength is used. For a logic operation it is important to have a spatial spread of impurities so that an interaction with one or two input ILMs can occur.

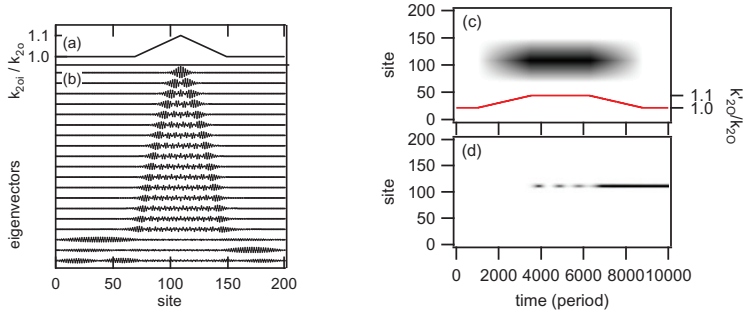

Fig. 1 (a) Spatial impurity pattern that is applied to manipulate an ILM. The disturbance is characterized by the ratio of the on-site impurity spring constant to the pure one. (b) Linear eigenvector patterns from the highest resonance frequency down to the 19-th mode. The top 16 island modes show a variety of localization behavior. (c) Impurity spatial and strength distribution as a function of time. (d) Result of the application of those impurities with fixed driver at 139 kHz. Energy density is plotted as a function of time: darker indicates larger energy. After the removal of the impurity, one ILM remains.

2.2 NOR logic operation

The Not-OR operation, or NOR for short, is defined as $\overline{A+B}$ in Boolean algebra where A and B are inputs. It gives 1 only when A=0 and B=0. Figure 2 shows the NOR logic operation through ILM simulations. The same impurity operation shown in Fig. 1 is applied with different initial conditions. The ILM appears in Fig. 2(a) where no initial ILM exists while in Figs. 2(b)-(d), the initial ILM is destroyed. If we code the absence or existence of an ILM as "0" or "1", then a NOR logic operation has been produced.

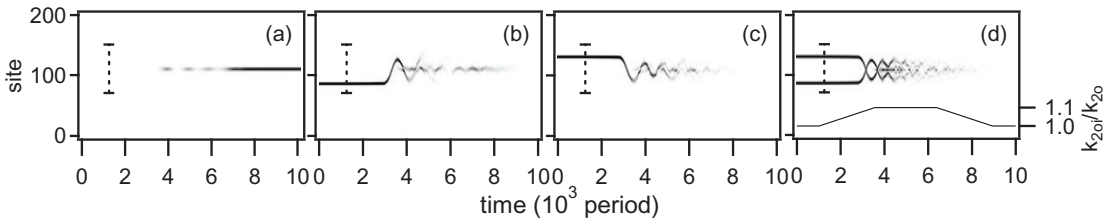

Fig. 2 NOR logic operation demonstrated in the array by simulations. The same impurity operation used in Fig. 1(a) was applied with different initial conditions. The vertical dashed line indicates the position of the distributed impurities. (a) When no initial ILM exists, one ILM is produced. (b) The initial ILM at site 87, and no ILM remains. (b) The initial ILM at site 131, and no ILM remains. (d) Initial ILMs at sites 87 and 131, and no ILMs remains. Time dependence of the impurity harmonic spring constant is shown in lower part of the panel (d).

In previous papers, we have noted that either an ILM is generated or no ILM appears in the perfect lattice depending on the relative phase of amplitude modulation (AM) at the time when the impurity mode strength is decreased.[19, 20] We separate the analysis of the operation into three stages: generation of the transient AM modulation at the initial stage, detection of the AM phase by removal of the defects at the final stage, and reversing the phase by interaction with the input-ILM at the middle stage. We will analyze these stages in the van der Pol phase plane, to be is introduced in the next section.

3. Analysis in the van der Pol phase plane

3.1. van der Pol phase plane for a driven nonlinear oscillator

The van der Pol phase plane diagram for a single driven nonlinear oscillator is well known. Here we consider the particular example of a Duffing oscillator for a single particle of the form

$$m\frac{d^2y}{dt^2}+\frac{m}{\tau}\frac{dy}{dt}+k_2y+k_4y^3=m\alpha\cos\Omega t\,. \tag{2}$$

It corresponds to Eq. (1) when the coupling to other particles is eliminated. To match the nonlinear lattice problem at hand the following parameters have been chosen: m=5.06×10^{-13} kg, k_2=0.2 N/m, k_4=5.0×10^8 N/m^3, τ=8.5ms and α=500 m/s^2. Figure 3(a) shows the driven response as a function of frequency. The harmonic resonance frequency is at 100 kHz. As the driving frequency increases beyond the harmonic value the amplitude continues to grow until it reaches the bifurcation point where the amplitude drops precipitously to a very small value. Decreasing the driving frequency from that value, as shown by the arrows, results in a second transition from a smaller to a larger amplitude state somewhat above but closer to the harmonic frequency.

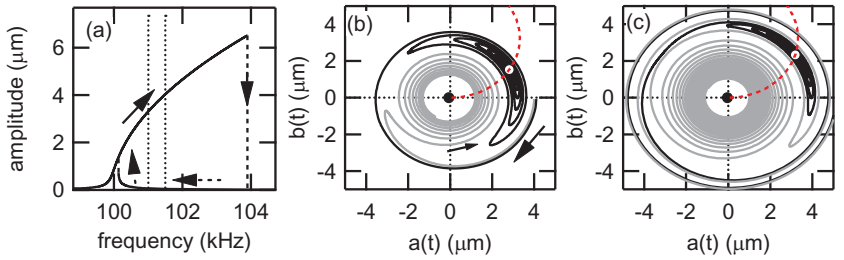

Fig. 3 (a) Response versus driving frequency of a nonlinear Duffing resonator. Arrows illustrate the hysteresis effect as the frequency is varied first to higher, then to lower frequencies. Vertical dashed lines (101 and 101.5 kHz) indicate particular driver frequencies for the van der Pol plane shown in (b) and (c). (b) Transient state trajectories leading to two attractors at 101 kHz. At this frequency, high and low amplitude stable periodic solutions exist. Gray curve is the trajectory that approaches the lower amplitude periodic state. Black curve represents the trajectory that leads to the large amplitude periodic state. Dashed curve starting from the origin indicate movement of the high amplitude attractor as a function of the driver frequency. It is near by the origin when the driver frequency is low as 99 kHz, and at the point marked by the open circle at 101 kHz. (c) The same figure as (b), but for 101.5 kHz driver frequency. The large amplitude state has moved along the dashed curve farther away from the origin compared to 101 kHz in (a).

For an approximate solution to Eq. (2) we assume the form

$$y(t)=a(t)\cos\Omega t + b(t)\sin\Omega t \tag{3}$$

The van der Pol phase plane plot of $b(t)$ versus $a(t)$ describes the transient states, which lead to the periodic states for a given driving frequency.[21] As an example consider the particular driving frequency 101 kHz represented by the dotted line (left) in Fig. 3(a). At this frequency, two stable solutions exist, one is for a high amplitude state and the other is for a low amplitude state. To keep track of the stability of the driven system it is helpful to present the results in a different form. Taking the starting condition as $a(0)=y(0)$=4.1×10^{-6} and 4.0×10^{-6} with $b(0)=y'(0)/\Omega$=0 the resulting phase plane is shown in Fig. 3(b). The black trace leads to the high amplitude attractor while the gray trace leads to the low amplitude one. For slightly larger driver frequency (101.5 kHz) the large amplitude stable state moves along the dashed

line farther from the origin. As the driving frequency changes the trajectories of each of the two attractors changes.

For the logic operation, the transient effect is important in the operation. The van der Pol phase plane is useful to illustrate how the transient state is different from the stable state, and how it approaches one of the attractors.

3.2. van der Pol phase plane for an impurity mode/ILM in a lattice

Although the nonlinear lattice system in question involves many degrees of freedom an ILM by its nature spans only a few lattice sites; moreover, the amplitude of this driver locked vibration is determined by the driver frequency, just as for a driven single Duffing oscillator. Since the (impurity mode/ ILM) vibration has a frequency very different from the plane wave spectrum form the expected solution will be similar to Eq. (3); namely,

$$x_{center}(t)=a(t)\cos\Omega t + b(t)\sin\Omega t. \quad (4)$$

Figure 4 presents both the amplitude of the top most impurity mode shown in Fig. 1(b), and the center site of the ILM as a function of the driver frequency. The top most trace, with arrows showing the direction of the frequency sweeps, is the highest frequency impurity mode. The small peaks at lower frequencies are due to lower frequency impurity modes, shown in Fig. 1(b).

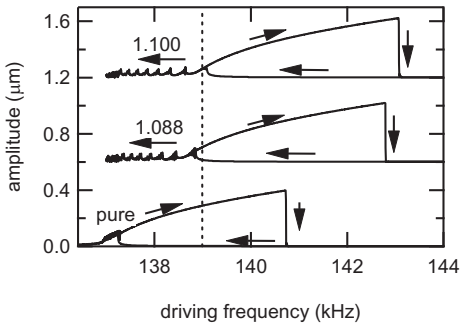

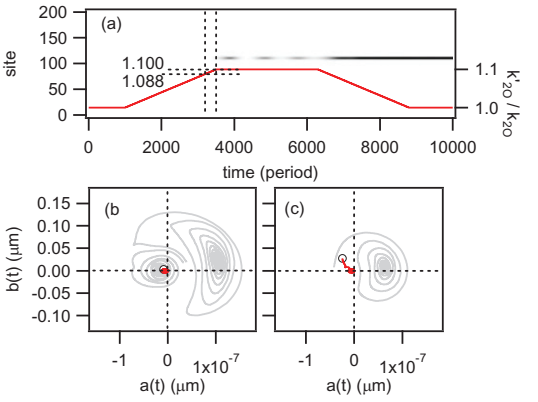

Fig. 4 Amplitude of the top impurity mode (upper and middle) and the ILM (bottom) as a function of the driver frequency. Numbers indicate the harmonic spring constant ratio at the center site, k_{2Oi}'/k_{2Oi}. Only the amplitude at the center site of the top most local mode is displayed here. The upper band limit for small oscillations of the pure lattice is at 137.1 kHz. The arrows show the frequency increasing from 139kHz to 144 kHz, then decreased to 137 kHz. The small multiple peaks in the upper and middle curves are due to island modes generated by impurities in Fig. 1(b). Bottom curve is for the ILM in a pure lattice. During the logic operation, the driver frequency is kept at 139 kHz throughout the paper (dashed vertical line).

Fig. 5 Initial stage of the NOR operation. (a) Vibrational energy density plot and impurity strength vs time profile (solid curve). Two horizontal dashed lines indicate the strengths of the time dependent van der Pol phase plane trajectories represented by the gray curves in panels (b) and (c). Impurity strengths in the two panels are 1.088 and 1.100, respectively. (b) Initial stage of the NOR operation. Resultant trajectory location (circle) for a state in panel (a) that starts at t = 0 and ends at t =3200 periods. Since the circle is essentially at the origin the impurity mode remains in the low amplitude state. (c) Resultant trajectory location (circle) for a state in panel (a) that starts at t = 0 and ends at t =3500 periods. The solid curve shows how it moves from the origin. Note that the attractor for the low amplitude state has disappeared and the state trajectory is now rotating around the one remaining impurity mode, large amplitude attractor. Associated with the rotation of this state is amplitude modulation of the vibrational energy density, shown in panel (a).

The vertical dashed line of Fig. 4 indicates a fixed driver frequency during the logic operations, and it coincides with the linear resonance frequency of the highest frequency impurity mode. For the pure lattice case (no impurity mode) the driver frequency is well above the top of the band frequency (137.1 kHz) and the ILM can exist with a large amplitude vibration or no-ILM with very small amplitude as shown by the bottom curve of Fig. 4. This is the first stage of the logic operation process. Both kinds of excitations behave similarly to a driven Duffing oscillator. For this reason it makes sense to use the van der Pol phase plane as an analysis tool for the ILM; even though, it is usually used to describe a single resonator. Both for the ILM and the impurity mode, the center motion of the excitation is described by the analog of Eq. (2) with the cosine driver at frequency Ω as a reference. Because the simulation model includes both the driver and damping, the system has attractor(s). A novel feature of this presentation scheme is that since the strength of the impurity mode changes with time the attractor(s) will also evolve with time.

3.3. Initial stage of the logic operation: generation of amplitude modulation

Consider Fig. 5(a) where the change in the linear impurity mode strength is shown as a function of time. The constant strength region is where the impurity mode frequency matches the driver frequency. The relatively sudden matching of the impurity resonance and the driver produces an amplitude modulation (AM) of the vibrational energy density as shown. The two horizontal dashed lines in Fig. 5(a) identify different impurity mode strengths of interest. To visualize how the vibrational state changes as a function of strength we now switch to the van der Pol plane representation and examine these two particular values. For a fixed impurity strength the vibration is completely governed by Eq. (1) and the display of *b(t)* vs *a(t)* starting from appropriate positions show how the transient states approach their respective attractors. The gray curves in Fig. 5(b) illustrate such a time dependent picture for the weaker of the two impurity strengths while Fig. 5(c) is for the stronger one. Note that the number of attractors changes in Figs. 5(b,c) from two to one as the impurity mode strength changes over a relatively small time interval. In Fig. 4 this corresponds to two solutions at the driver frequency for the lower strength impurity mode (middle curve) but one solution for the full strength of the defect (upper curve).

If one now calculates the end point of the time dependent trajectory from t=0 to t=3200 periods for the variable strength show in Fig. 5(a) the result is the open circle in Fig. 5(b), which is very close to the low amplitude attractor location found for the earlier static strength calculation. If one carries out the same calculation for the range from t=0 to t= 3500 periods one obtains the open circle shown in Fig. 5(c). Now there is only one attractor available and it is located at a large amplitude location. After the low amplitude attractor disappears, the trajectory commences to rotate around, and homes in on, the remained one. Because this remaining attractor is far from the origin, and because the low amplitude one was near the origin, a spiraling motion begins with a large radius, as represented by the solid line in Fig. 5(c). The resulting signature is the large amplitude modulation of the vibrational energy given by the dashed pattern in Fig. 5(a).

3.4. Final stage of the operation: detection of the AM phase

The last stage of the operation is to create or destroy and ILM. This is done by detecting the AM phase and using this phase information for the creation or destruction process. To see how the AM phase determines the end result, we show in Figs. 6(a, b) the effect of changing the phase by one half period. Fig. 6(a) is a repeat of the data in Fig. 5(a) while in Fig. 6(b) the removal of the impurity strength profile is started one half AM period earlier. No ILM appears at long times.

Figure 6(c) displays the entire van der Pol phase path for the ILM development in Fig. 6(a) when the impurity mode frequency is varied from ω_0/ω_m=1.00 $\rightarrow$ 1.013 $\rightarrow$ 1.00, caused by the time-dependent

defect strength k_{2Oi}'/k_{2Oi}=1.00 → 1.10 → 1.00, where ω_0 is the impurity mode frequency and ω_m is the top band mode frequency (137.1kHz). The path starts from the origin and spirals around the impurity mode attractor over the constant strength period. When the impurity mode strength decreases the attractor, represented by the thick arc, moves to a larger amplitude location while the impurity mode evolves into an ILM, represented by the oscillatory track, which follows the, now ILM, attractor.

Figure 6(d) shows what happens to the trajectory when the AM phase associated with the impurity mode is decreased one half period sooner. The initial spiral is the same as for Fig. 6(c) because the growth of the impurity strength is the same in both cases. But now the trajectory no longer follows the moving attractor and instead collapses back to the small amplitude state. Depending on the relative phase of the amplitude modulation at the time when the impurity mode strength is decreased (a) shows the change into the large amplitude ILM while (b) does not.

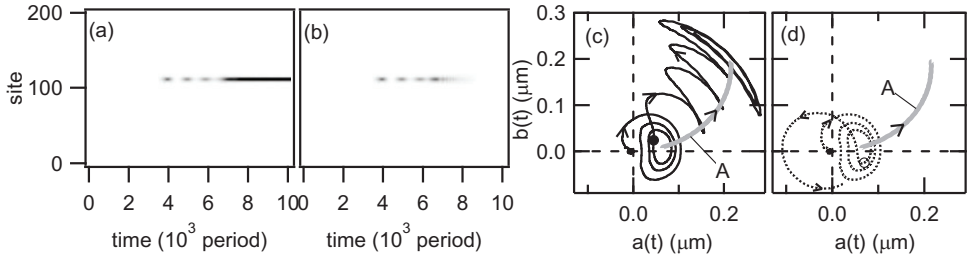

Fig. 6(a) Vibrational energy density plot ends with a large amplitude ILM, by the NOR impurity operation. (b) If the impurities are removed a half period of the AM oscillation earlier than in case (a), no ILM is formed. (c) Complete van der Pol phase path for the generation of the large amplitude ILM in (a), when the impurity mode frequency is varied from ω_0/ω_m=1.00 → 1.013 → 1.00, where ω_0 is the impurity mode frequency and ω_m is the linear top most frequency of the pure lattice. The initial spiral path is that of the driven impurity mode into the constant strength time interval. The large oscillatory track shows how the vibrational excitation follows the moving attractor (solid arc) as the impurity mode strength is decreased and an ILM is produced. (d) The dashed curve illustrates the corresponding path for the trajectory in the no-ILM case. The thick arc indicated by "A" in (c, d) shows the time dependent attractor for the ILM.

To better understand this switching process we now examine the last part of the two paths where ω_0/ω_m=1.013 → 1.00 since the end result strongly depends on the timing of the impurity mode removal relative to the phase of the AM. These van der Pol plots are shown in Fig. 7. With the impurity mode at full strength the AM impurity mode path is given by the solid curve in Fig. 7(a), starting at the bottom of the figure and circling around the fixed attractor center, identified by the triangle. By starting at the open circle position the strength of the impurity mode begins to decrease and the resultant path for this no-ILM is represented by the dashed curve that peels off to the left, away from that particular attractor. The time dependence of the center of the no-ILM attractor is identified in the figure. If, on the other hand, the strength of the impurity mode begins to decrease at a later time, represented by the solid dot then the trajectory peels off to the right, moving in the same direction as the time dependent ILM attractor, as shown. To follow the paths relative to the attractors, their basins are calculated for three different impurity mode frequencies, the maximum frequency plus two smaller values: ω_0/ω_m=1.013, 1.011, 1.010. Figure 7(b, c, d) are for the ILM case. The solid dot represents the ILM path position for that particular local mode frequency and the open circles in Fig. 7(e, f, g) represent the no-ILM positions for the same local mode frequencies. In each case the path just follows the spiral orbit towards its attractor located at that particular time (local mode frequency). Another interesting feature is the appearance of two attractors as the local mode frequency decreases. This illustrates how the impurity mode changes to an ILM. Finally compare the solid and open circles of Fig. 7(c, f) with those in Fig. 7(d, g). Initially, both trajectories are in the same basin of the high amplitude trapped-ILM state. However, at ω_0/ω_m=1.010, the solid circle

remains in the same basin while the open circle is in the other basin, of the lower amplitude (no ILM) state.

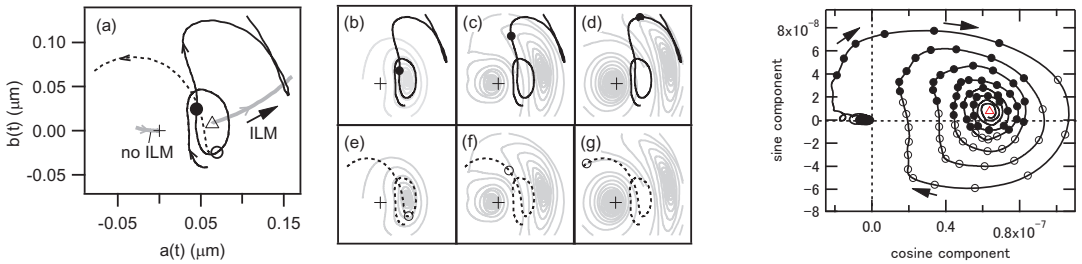

Fig. 7 (a) Trajectories of the ILM and the no ILM states as a function of the initial decent time of the impurity mode frequency. Origin is marked by "+". The open circle indicates the initial decent time for the no ILM case (dashed curve). The solid dot indicates the corresponding starting time for the ILM case. The one attractor located at the triangle position evolves into two attractors shown in gray. Frames (b-g) Evolution of the attractor basins with changing impurity mode frequency (gray spirals). Frames (b,c,d): Each solid circle is a point on the trajectory of the solid curve in panel (a) at impurity mode frequency ω_0/ω_m=1.013, 1.011, 1.010, respectively. These solid circles are superimposed on the spiral orbit basins leading toward the attractor(s) for the same impurity mode frequencies. Frames (e,f,g): The same evolution of the trajectories, using open circles for the same three frequency ratios, for the no-ILM dashed curve in panel (a).

Fig. 8 End results mapped on the van der Pol phase plane. Solid curve shows the excitation trajectory if the impurities are introduced as shown in Fig. 5(a) but are not removed. It approaches to the impurity attractor (triangle) continuously following the spiral. When the trajectory is far from the origin, the AM is large. As the trajectory approaches the attractor, the AM becomes small. To see the phase dependence of the end results, the initiation of the impurities is started at each marker. Solid and open circles indicate ILM and no-ILM end results, respectively. As long as the spiral radius is large, the end result depends on the orbit position at initiation. Roughly if the orbit is in the upper half plane an ILM results, i.e., if initiation starts when the amplitude is increasing, the ILM remains. For a small radius, an ILM state is always found.

So far, only the two removal points shown in Fig. 7(a) have been tested. The next step is to determine the dependence of the end point result on the removal time of the impurity mode. The solid curve shown in Fig. 8 is the trajectory from t=0 up to a constant impurity strength. As time progresses the impurity mode spirals into the attractor. Removal times tested along this trajectory are identified by the solid and open circles, solid circles give ILM states while the open circles, no ILM states. For a large spiral radius the end result is either an ILM or no-ILM depending on the relative position to the attractor. Roughly, if the removal starts in the upper half plane the ILM remains. This corresponds to a time duration when the amplitude is increasing in one period of the AM. If the modulation is too small the energy is always in the ILM state so there is no way to switch it off.

One can carry out the inverse onsite process of starting with an ILM at the center site and either destroying it or retaining it as long as AM modulation produced by the force constant perturbation is sufficiently rapid. We find that the rise time used in Fig. 5(a) is too slow to generate the necessary AM to make this branching possible but decreasing the rise time from 2500 periods to 500 periods is sufficient to permit the inverse process to occur.

3.5. Interaction stage of the logic operation: modifying the AM phase

Figure 2(b) illustrates that another way to obtain a large AM so that an ILM can either be destroyed or retained is to have the ILM off center with respect to the impurity array. Since ILMs are dynamical impurities they can be located anywhere in the pure lattice if they are sufficiently separated from one another. For example, the minimum distance for noninteracting ILMs for the simulation conditions given in Table II of Ref. [16] is 12 lattice constants. If an impurity is added to the lattice sufficiently close to an

ILM with an impurity mode frequency between the top of the plane wave spectrum and the driver frequency, then the impurity mode attracts the ILM. The critical distance for the attractive interaction is 32 lattice constants for the simulations.

An initial ILM, as shown in Figs. 2(b)-(c), is attracted by the impurity array. Because the distribution of impurities is smooth the attracted ILM passes through the center of the distribution and oscillates about it with decreasing range. Figure 9(a) shows the destruction of the ILM while Fig. 9(b) shows the same initial condition but initiation time of the impurity removal is half AM period earlier. As in Figs. 6(a,b), the end results are opposite to each other. Thus, phase inversion of AM is a general property. During this process the impurity mode grows and interacts with the input ILM giving rise to strong AM. In addition the translation of the ILM excites island modes, shown in Fig. 1(b), and their vibrations complicate the response of the central site. Their van der Pol plots are presented in Figs. 9(c,d). These trajectories are very complex; however, the similarities between Figs. 9(d) and 6(c) and also between Figs. 9(c) and 6(d) are evident. Like Figs. 6(c,d) the end result depends on whether the impurity removal time is in the upper or lower half plane.

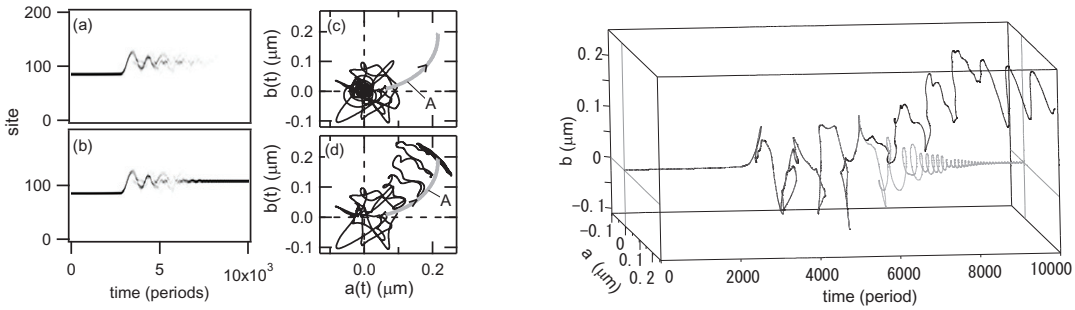

Fig. 9 (a) Destruction of an ILM using an impurity array with the off-centered initial ILM at site 87 while the impurities are centered at site 109. This is the same figure as Fig. 2(b). (b) Translation of an ILM using an impurity array. Initiation of the removal time was one half AM period earlier than in (a). The result is inverted from (a). (c) Van der Pol plot of the center impurity site for panel (a). Solid curve is the trajectory over the entire time interval. Thick gray curve is the attractor path. (d) The van der pol plot for panel (b).

Fig. 10 The complete 3-D trajectories showing the van der Pol plane versus time. Black curve is for panel (b) and gray curve is for panel (a). Those curves start apart with each other at t=5900 period.

Another way to view the two different trajectories is to display the time dependence of the van der Pol plot in 3-D. Figure 10 displays a 3D plot of the van der pol plane as a function of time for the two cases just described. The initial complexity in the 2-D plot simplifies beyond t=5900 period. The two curves separate. The gray one, the no ILM state, spirals back to the origin while the black curve approaches the high amplitude ILM state.

4. Summary

From this investigation we conclude that the AM of the time dependent ILM/impurity mode strength is the key element required to switch an ILM between two different states. When these developments are represented in the van der Pol plane detailed dynamics become evident. The production of a driven ILM due to the action of the time dependent ILM/impurity mode frequency is particularly enlightening in that the sudden disappearance of the low amplitude attractor is directly connected with the production of large AM when the impurity mode frequency approaches the driver frequency. The impurity mode trajectory

then rotates around the impurity attractor with a large radius. Upon decreasing the impurity mode frequency at a specific time the excitation can either follow the large amplitude attractor and give rise to a stable ILM or collapse back to the small amplitude attractor depending on the AM at that time. The key is that when the removal starts, because of the motion of the attractor, the orbit either crosses the border of the basin to the low amplitude state, if the orbit is in the lower half plane; or if it is in the upper half plane then approaches the basin of the high amplitude attractor.

Destroying an ILM by varying the time dependent impurity mode strength produces a more complex trajectory. To obtain the large AM the location of the impurity mode center is shifted with respect to the ILM center. When the impurity mode strength increases the ILM is attracted to it and this translational motion gives rise to AM at the impurity mode center. We show that once again depending on the AM phase the end result is either an ILM or no ILM. In terms of the van der Pol plots the orbit either crosses the border of the basin to the low amplitude state, if the orbit is in the lower half plane, or the converse. The trajectory in the phase plane of a driven ILM can be understood in terms of motion of attractors controlled by application of a time-depended impurity strength.

Acknowledgments

The research was supported by Grant-in-Aid for challenging Exploratory Research (21656022). BEH and AJS were supported by NSF-DMR-0906491.

References

[1] S. W. Shaw, B. Balachandran, J. of System Design and Dynamics **2**, 611(2008).

[2] J. F. Rhoads, S. W. Shaw, and K. L. Turner, J. of Dynamic Systems, Measurement, and Control, **132**, 034001(2010).

[3] F. C. Hoppensteadt and E. M. Izhikevich, IEEE Trans. on Circuits and Systems I: Fundamental Theory and Appl. **48**, 133(2001)

[4] A. J. Sievers and S. Takeno, Phys. Rev. Lett. **61**, 970 (1988)

[5] A. J. Sievers and J. B. Page, "Unusual anharmonic local mode systems" in "Dynamical Properties of Solids: Vol. 7, Phonon Physics, The Cutting Edge", G. K. Norton and A. A. Maradudin, eds., (North Holland, Amsterdam, 1995), p 137.

[6] D. K. Campbell, S. Flach, and Y. S. Kivshar, Physics Today **57**, 43 (2004).

[7] S. Flach and C. R. Willis, Phys. Repts. **295**, 182 (1998).

[8] S. Flach and A. Gorbach, Phys. Repts. **467**, 1 (2008).

[9] A. J. Dick, A. J. Balachandran, and C. D. Mote, Nonlin. Dyn. **54**, 13 (2008).

[10] T. Rössler and J. B. Page, Phys. Lett. A, **204**, 418 (1995)

[11] M. Sato, B. E. Hubbard, A. J. Sievers, B. Ilic, D. A. Czaplewski and H. G. Craighead, Phys. Rev. Lett. **90**, 044102 (2003)

[12] Q. Chen, L. Huang, Y.-C. Lai, and D. Dietz, Chaos **19**, 013127 (2009).

[13] J. Wiersig, S. Flach, and K. H. Ahn, Appl. Phys. Lett. **93**, 222110 (2009).

[14] E. Kenig, R. Lifshitz, and M. C. Cross, Phys. Rev. **E 79**, 026203 (2009).

[15] E. Kenig, B. A. Malomed, M. C. Cross, and R. Lifshitz, Phys. Rev. **E 80**, 046202 (2009).

[16] M. Sato, B. E. Hubbard, and A. J. Sievers, Rev. Mod. Phys., vol. **78**, pp. 137-157,(2006).

[17] M. Sato, B. E. Hubbard, A. J. Sievers, B. Ilic, and H. G. Craighead, Europhys. Lett. **66**, 318 (2004)

[18] J. Fajans and L. Friedland, Am. J. Phys. **69** , 1096-1102 (2001).

[19] M. Sato, N. Fujita and A. J. Sievers, DCDS-S, vol. **4**, No.5, pp. 1287 - 1298(2011).

[20] M. Sato, N. Fujita, S. Imai, S. Nishimura, Y. Hori and A. J. Sievers, AIP Conference Proceedings v. **1339**, pp 118 (2011).

[21] D. W. Jordan and P. Smith, "Nonlinear Ordinary Differential Equations", 4th ed. (Oxford University Press, 2007), Ch. 7.